Mem. Natl Inst. Polar Res., Spec. Issue, **55**, 87–104, 2001

New evidence for prograde metamorphism and partial melting of Mg-Al-rich granulites from western Namaqualand, South Africa

Yoshikuni Hiroi[1], Tomokazu Hokada[2], Masaaki Beppu[1], Yoichi Motoyoshi[2], Toshiaki Shimura[3], Masaki Yuhara[4], Kazuyuki Shiraishi[2], Geoffrey H. Grantham[5] and Mike W. Knoper[6]

[1]*Department of Earth Sciences, Faculty of Science, Chiba University, 1-33, Yayoi-cho, Inage-ku, Chiba 263-8522*
[2]*Department of Crustal Studies, National Institute of Polar Research, Kaga 1-chome, Itabashi-ku, Tokyo 173-8515*
[3]*Department of Geology, Faculty of Science, Niigata University, 2-8050, Ikarashi, Niigata 950-2181*
[4]*Department of Earth System Science, Faculty of Science, Fukuoka University, 8-19-1, Nanakuma, Jonan-ku, Fukuoka 814-0180*
[5]*Council for Geoscience, P/Bag X112, Silverton 0127, South Africa*
[6]*Department of Geology, Rand Afrikaans University, PO Box 524, Auckland Park 2006, South Africa*

Abstract: Cordierite-phlogopite gneiss with spectacular coarse pseudomorphs of sillimanite after andalusite occurs as a kind of Mg-Al-rich rock in the Dabeeb-Hytkoras area of the granulite-faces western Namaqualand Metamorphic Complex. The sillimanite pseudomorphs are always fringed by spinel-cordierite coronas, which, in turn, are surrounded by cordierite mono-mineral zones. The spinel-cordierite coronas include minor amounts of sapphirine, corundum and rutile. The matrix comprises mainly cordierite and phlogopite with minor plagioclase and orthopyroxene plus a trace of quartz. Orthopyroxene is often replaced partially by symplectitic intergrowths of phlogopite and quartz. The modes of occurrence and chemical compositions of minerals indicate that the rock followed a prograde metamorphic *P-T* path from the andalusite to the sillimanite stability fields and a subsequent isobaric cooling path and that partial melting took place during granulite-facies metamorphism resulting in its present geochemical character.

key words: Namaqualand, granulite facies, cordierite-phlogopite gneiss, sillimanite pseudomorph after andalusite, spinel-cordierite corona, partial melting

1. Introduction

The Namaqua Metamorphic Complex (Province) of South Africa is one of the well-documented low-pressure high-temperature type metamorphic terranes, and an anticlockwise *P-T-t* path is established there (*e.g.*, Waters, 1989; Raith and Harley, 1998). However, there remains uncertainty concerning the prograde *P-T* path followed by granulites, especially those in the Springbok-Garies area, where Mg-Al-rich gneisses occur as minor components of supracrustal sequences dominated by quartzo-feldspathic

gneisses (Clifford *et al.*, 1975b, 1981; Waters and Moore, 1985; Waters, 1986b; Moore, 1989). The origin of such Mg-Al-rich rocks is still controversial: whether the geochemical character results from metamorphic or premetamorphic processes (*e.g.*, Spear, 1993). In this paper we present petrologic data on a newly found granulite-facies Mg-Al-rich rock from the western Namaqualand Metamorphic Complex in order to overcome the uncertainty concerning the *P-T* path and to obtain some insight into the processes that produce Mg-Al-rich rocks.

2. Geologic setting

The Namaqualand Metamorphic Complex forms part of the Mid-Proterozoic (*c.* 1.3–1.0 Ga) Namaqua-Natal Mobile Belt that surrounds the Archean Kaapvaal Craton in the west and south (*e.g.*, Jacobs *et al.*, 1993). It is divided into three tectonically distinct subprovinces: the Bushmanland, the Gordonia and the Richtersveld Subprovinces (Joubert, 1986a, b; Thomas *et al.*, 1994). The Springbok-Garies area where we carried out geologic survey and sample collection in 1998 and 1999 is part of the Bushmanland Subprovince and is underlain by granulite-facies metamorphic rocks of early- to mid-Proterozoic supracrustal rock origin as well as syn- to late-kinematic granitic intrusives (*e.g.*, Clifford *et al.*, 1995; Robb *et al.*, 1999). The supracrustal rocks are composed mainly of quartzite and pelites accompanied by basic, Mg-Al-rich, and oxide-rich varieties. Several ductile deformation events have been established (Joubert, 1971, 1986a, b). Major syn-metamorphic deformation D2 is normally developed as a penetrative subhorizontal foliation or metamorphic layering combined with formation of isoclinal to recumbent F2 folds with east-west trending axes.

Metamorphic studies of supracrustal rocks have defined an E-W symmetry of metamorphic zonation (Waters, 1986a, 1989) (Fig. 1). A central zone is characterized by upper granulite-facies metamorphism: hercynitic spinel + quartz and rare osumilite-bearing assemblages occur in metapelites (Waters, 1986a, 1991; Nowicki *et al.*, 1995). The central zone grades into lower granulite-facies and upper amphibolite-facies zones toward the north and south (Fig. 1). The characteristic mineral assemblages of the lower granulite-facies zone are cordierite + garnet + K-feldspar + quartz in metapelites and orthopyroxene + clinopyroxene + hornblende + plagioclase in metabasites, whereas that of the upper amphibolite-facies zone is sillimanite + biotite + K-feldspar + quartz in metapelites (Waters, 1986a, 1989, 1990). Partial melting of metapelites by dehydration of biotite is observed at the amphibolite-granulite facies transition and in the higher-grade area (Waters and Whales, 1984; Raith and Harley, 1998).

P-T estimates for the western Namaqualand Metamorphic Complex show considerable scatter. Estimates for the central upper granulite-facies zone vary between 800 and 860°C at *c.* 7 kbar (Zelt, 1980); >800°C at *c.* 5 kbar (Waters, 1986a); 800–860°C at 4–6 kbar (Waters, 1989), and 870°C at 5 kbar at the osumilite locality (Nowicki *et al.*, 1995). The lower granulite-facies zones exhibit lower temperature conditions at similar or slightly lower pressures (750–800°C at 3–6.5 kbar) and the upper amphibolite-facies zones imply 650–700°C at 3.5–4.5 kbar (Waters, 1989).

We visited the kornerupine locality K2 of Waters and Moore (1985) in the lower granulite-facies Dabeeb-Hytkoras area (Fig. 1), where the supracrustal rocks comprise

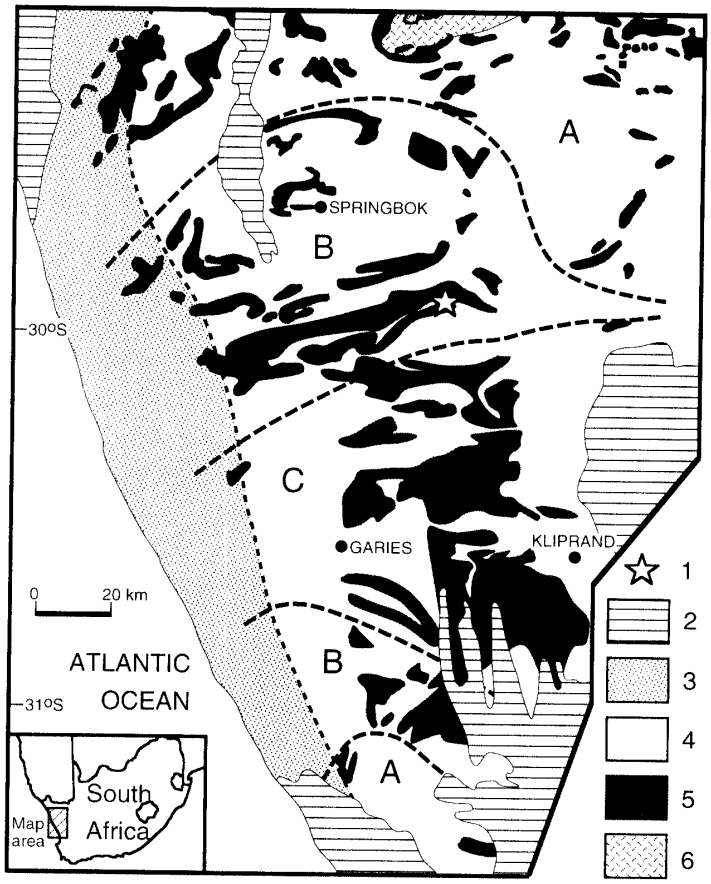

Fig. 1. Simplified geologic map of western Namaqualand showing (1) locality of studied cordierite-phlogopite gneiss with sillimanite pseudomorphs after andalusite, the occurrences of (2) Late Precambrian to Karoo cover, (3) the Namaqualand Metamorphic Complex reworked during the Pan African event, (4) granitic intrusive rocks of the Namaqualand Metamorphic Complex, (5) supracrustal enclaves of the Namaqualand Metamorphic Complex, and (6) the Vioolsdrif Suite and Orange River Group (1700–2000 Ma), and the Namaqua metamorphic zonation; A=upper amphibolite facies; B=a cordierite-garnet subzone of granulite facies; C=a spinel-quartz subzone of granulite facies. Data sources: Waters (1986a, 1989, 1990, 1991), Andreoli et al. (1994).

quartzo-feldspathic biotite gneisses and leucogneisses with minor interbedded two-pyroxene gneisses, sillimanite-cordierite-garnet gneisses, quartzites, and garnet-clinopyroxene calc-silicate rocks. Cordierite-phlogopite and cordierite-orthopyroxene gneisses, part of which include kornerupine, sapphirine, spinel, corundum and/or sillimanite, are also found as Mg-Al-rich thin layers in close association with two-pyroxene gneisses and sillimanite-cordierite-garnet gneisses (Waters and Moore, 1985; Waters, 1986b; Moore and Waters, 1990).

3. Petrography

Around K2 of Waters and Moore (1985) in the Dabeeb-Hytkoras area we collected many specimens of granulites with variable chemical compositions (*e.g.*, Hokada *et al.*,

2001). In addition to those from outcrops, we obtained boulder specimens, one of which (*99082501X*) is the target of this study. It is coarse-grained, reddish brown cordierite-phlogopite gneiss with spectacular coarse (up to 4 cm long) pseudomorphs of sillimanite after andalusite (Figs. 2 and 3). The rock is divided into two parts: silica-undersaturated sillimanite pseudomorphs fringed by spinel-cordierite coronas and the silica-saturated cordierite-phlogopite matrix, which are separated from each other by cordierite monomineral zones surrounding the spinel-cordierite coronas (Figs. 3 and 4).

The coarse sillimanite pseudomorphs comprise several sectors that consist of a mosaic of mostly subparallel prisms of sillimanite (Fig. 3). The prismatic habit of the former andalusite crystals is well preserved in the low-strain part (Fig. 2a). Orientation of (010) and [001] of sillimanite prisms is correlated to the outlines of the former andalusite (Fig. 3). The sillimanite mosaic may have been formed by polynuclear recrystallization from andalusite (*e.g.* Rosenfeld, 1969). Minor amounts of corundum,

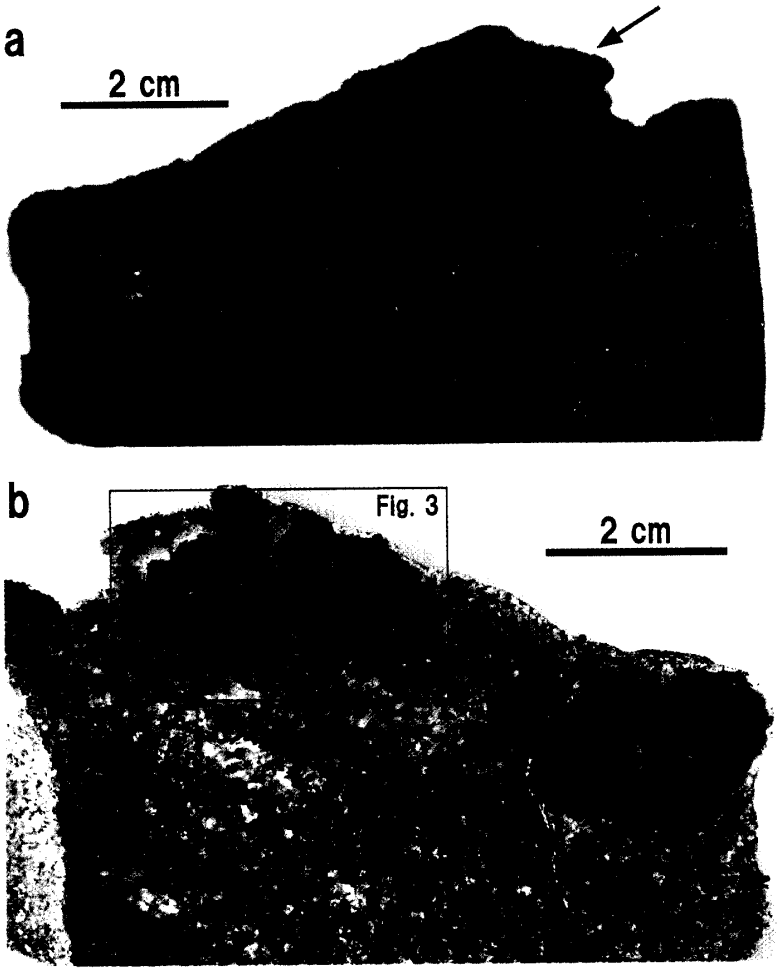

Fig. 2. Close-up view of studied cordierite-phlogopite gneiss with sillimanite pseudomorphs after andalusite. (a) Reddish brown weathered surface of cordierite-phlogopite gneiss with black, knobby, spectacular coarse pseudomorphs of sillimanite after andalusite. Note the well-preserved prismatic habit of the former andalusite crystals (arrow). (b) Polished surface of cordierite-phlogopite gneiss showing sillimanite pseudomorphs rimmed by black spinel-cordierite coronas.

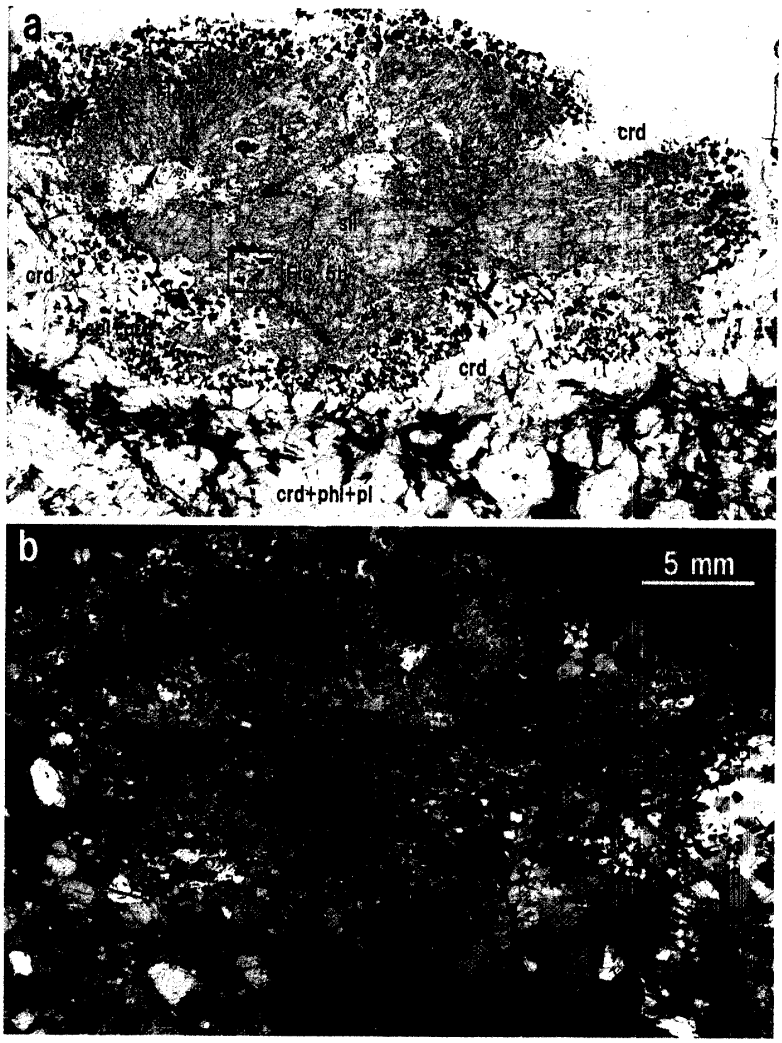

Fig. 3. Photomicrographs of sillimanite pseudomorph after andalusite in Sp. 99082501X. Note that the pseudomorph comprises several sectors consisting of a mosaic of sillimanite prisms, and is rimmed by spinel-cordierite coronas which, in turn, are surrounded by cordierite mono-mineral zones. The cordierite mono-mineral zones separate the corundum-bearing silica-undersaturated sillimanite pseudomorph including the spinel-cordierite coronas from the quartz-bearing silica-saturated matrix. (a) Plane-polarized light. (b) Crossed polars.

sapphirine, spinel, cordierite, phlogopite, rutile, magnetite, ilmenite, apatite, monazite and zircon occur within the sillimanite pseudomorphs and are in direct contact with each other. Corundum is often euhedral and contains inclusions of fibrolite (Fig. 5), indicating that its growth postdated the prograde transformation of andalusite to sillimanite. It is sometimes accompanied by hematite of possible exsolution origin. Sapphirine is commonly anhedral (skeletal), being intergrown with cordierite, sillimanite, spinel and phlogopite (Fig. 5a, b). Spinel sometimes forms symplectite with cordierite to replace sillimanite partially (Fig. 5c).

The coronas fringing the sillimanite pseudomorphs consist mainly of spinel and cordierite with minor corundum, sapphirine, phlogopite, magnetite, rutile, ilmenite,

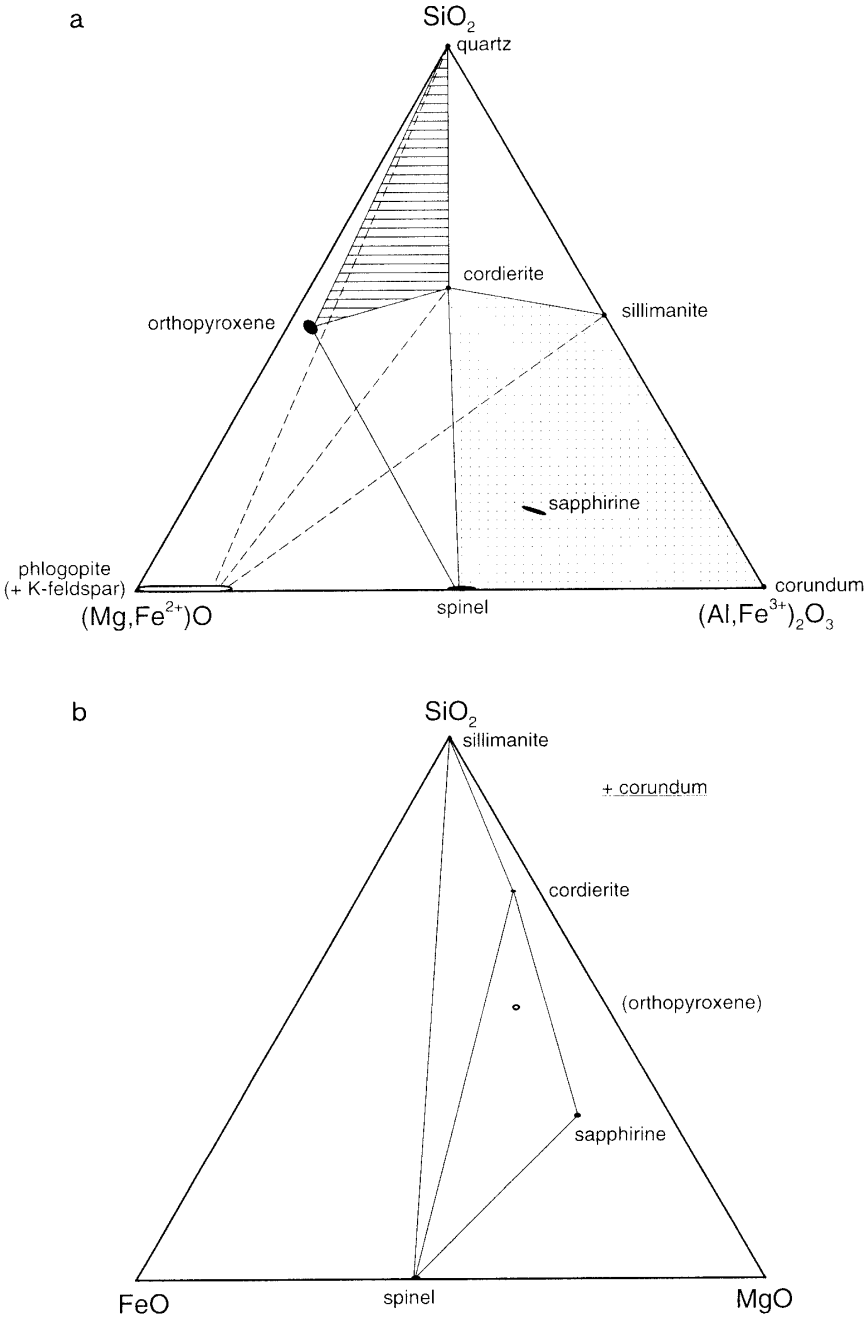

Fig. 4. Triangular diagrams showing phase relations observed in Sp. 99082501X from the Namaqualand Metamorphic Complex. (a) The system SiO_2-$(Mg,Fe^{2+})O$-$(Al, Fe^{3+})_2O_3$ (mol%) showing two portions corresponding to the silica-undersaturated sillimanite pseudomorphs after andalusite (dotted) and silica-saturated matrix (ruled). Phlogopite projected from K-feldspar is also shown for reference, though K-feldspar is absent in the rock. (b) Projection from corundum onto the SiO_2-FeO-MgO plane in the system SiO_2-MgO-FeO-Al_2O_3, showing phase relations in the silica-undersaturated sillimanite pseudomorphs and surrounding coronas. Orthopyroxene in the matrix is also plotted for reference only.

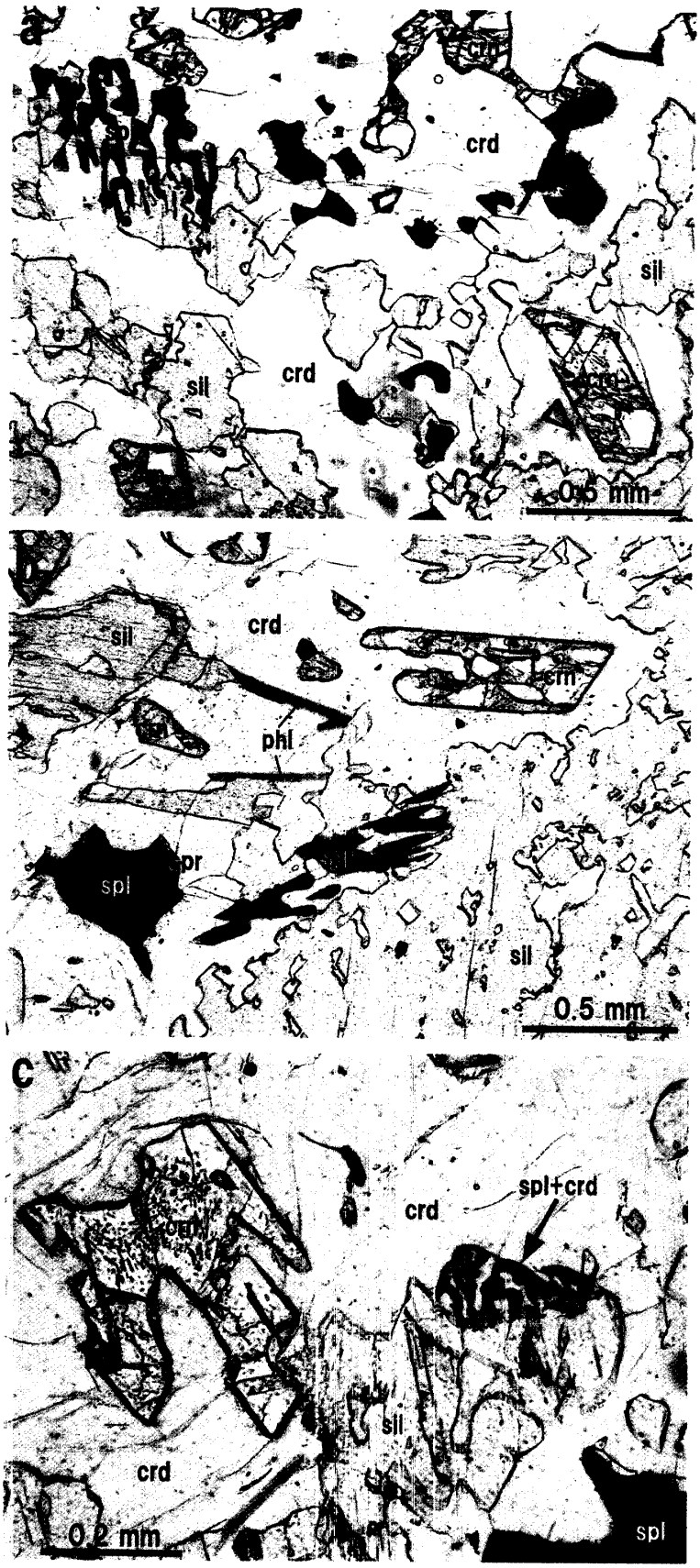

Fig. 5. Photomicrographs showing textural relations among sapphirine, spinel, corundum, sillimanite and cordierite in sillimanite pseudomorphs and spinel-cordierite coronas. (a) and (b) Spongy sapphirine is intergrown with sillimanite and cordierite. Corundum is often euhedral and contains inclusions of fibrolite. Phlogopite is also present in a small amount. Note yellow haloes around tiny inclusions of monazite and zircon. (c) Sillimanite is partially replaced by spinel-cordierite symplectite (arrow).

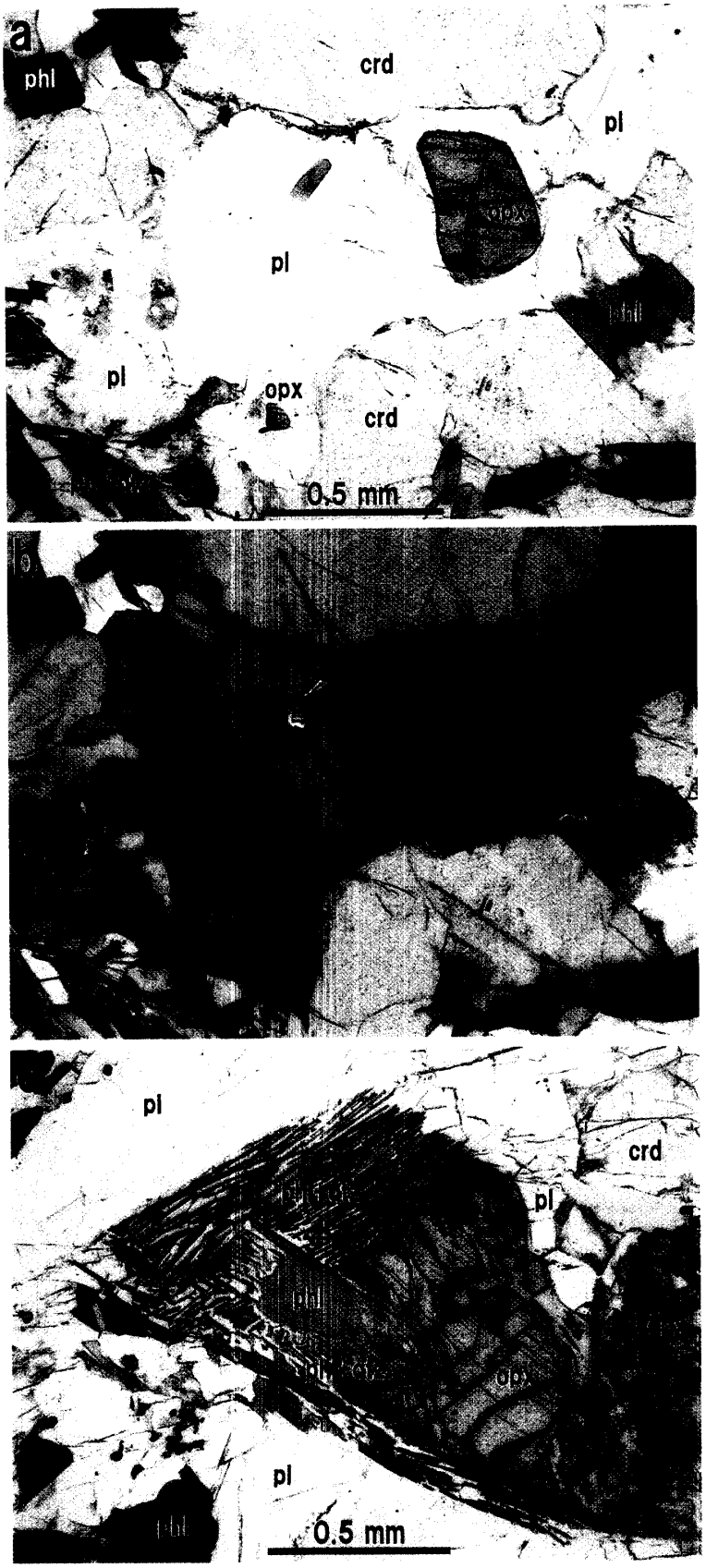

Fig. 6. Photomicrographs showing modes of occurrence of orthopyroxene in the matrix. (a) and (b) Anhedral orthopyroxene is completely surrounded by plagioclase and separated from cordierite which is characterized by its dusty appearance compared to clear plagioclase. (c) Orthopyroxene is partially replaced by symplectitic intergrowths of phlogopite and quartz.

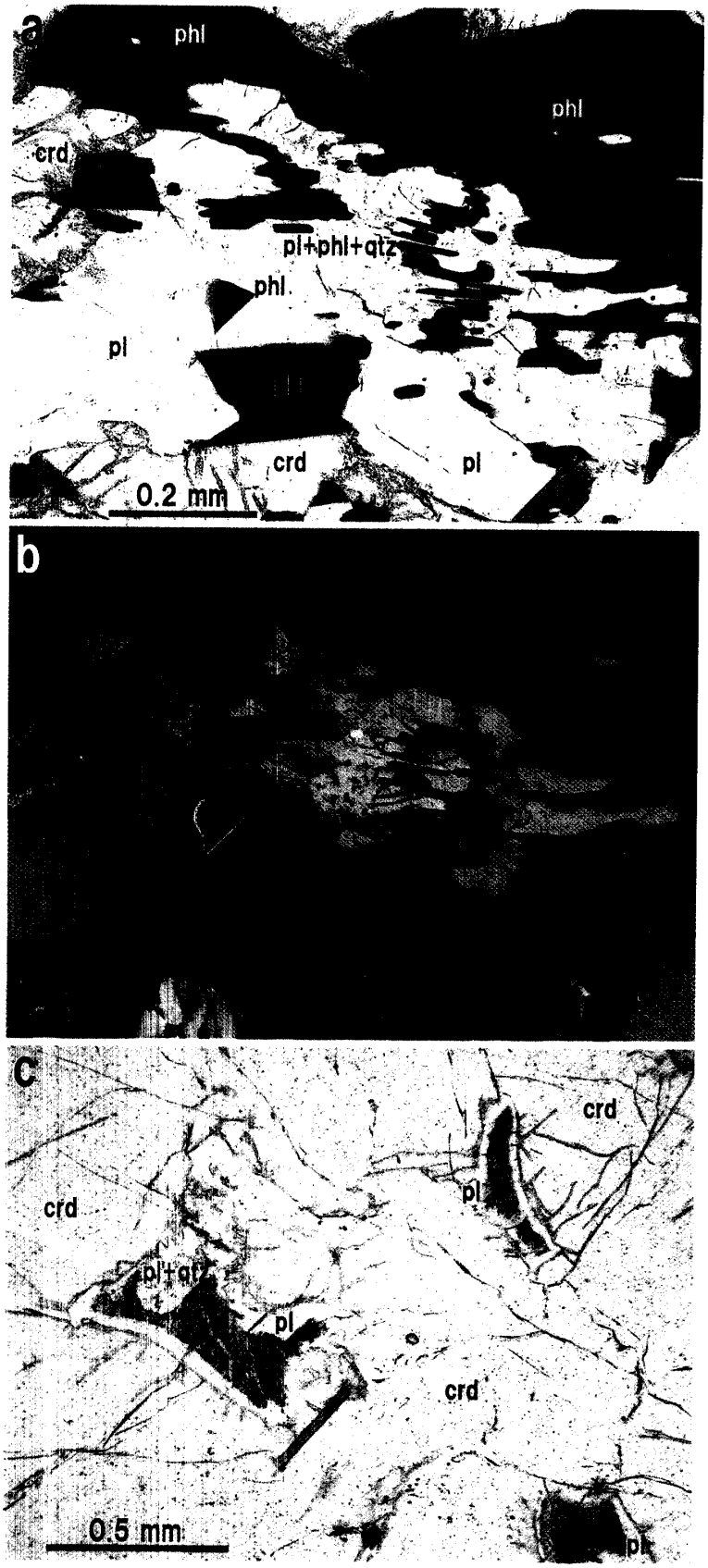

Fig. 7. Photomicrographs showing modes of occurrence of phlogopite and plagioclase in the matrix. (a) and (b) Two distinct modes of occurrence of plagioclase: relatively coarse grains almost free of inclusions, and amoebic grains containing inclusions of fine-grained phlogopite and vermicular quartz. (c) Interstitial plagioclase grains with dusty interiors. Myrmekitic intergrowth with quartz is also seen.

apatite, monazite and zircon. The modes of occurrence of these minerals are essentially the same as those within the sillimanite pseudomorphs except for the absence of sillimanite in the coronas. The spinel-cordierite coronas are always surrounded by cordierite mono-mineral zones (Fig. 3), which are the boundary between the silica-undersaturated and silica-saturated parts of the rock (Fig. 4a). Yellow halos around tiny inclusions of rutile, monazite and zircon are seen in cordierite.

The matrix comprises cordierite and phlogopite with subordinate plagioclase and minor orthopyroxene, quartz, ilmenite, apatite, monazite and zircon. To the naked eye, most cordierite grains are orange-yellow because of yellow halos around numerous minute inclusions of monazite and zircon. It is noteworthy that subhedral to anhedral orthopyroxene is always surrounded by plagioclase and separated from cordierite (Fig. 6a, b). Orthopyroxene is often replaced partially by symplectite of phlogopite and quartz (Fig. 6c). Phlogopite shows three modes of occurrence: (1) as coarse grains showing weak preferred orientation and traces of deformation (Figs. 3 and 7a, b); (2) as fine-grained inclusions in plagioclase which contains vermicular quartz (Figs. 7a, b); and (3) as grains intergrown with quartz to form symplectites that replace orthopyroxene (Fig. 6c). Plagioclase also shows three distinct modes of occurrence: (1) as relatively coarse grains similar to major cordierite (Fig. 6a, b), (2) as grains containing fine inclusions of phlogopite and quartz (Fig. 7a, b) and (3) as interstitial grains that include dusty interiors (Fig. 7c). Quartz occurs only in a trace amount either as vermicular grains contained in plagioclase (Fig. 7a, b) or as those forming symplectites with phlogopite after orthopyroxene (Fig. 6c).

4. Mineral chemistry

Minerals were analyzed with an energy-dispersive type electron microprobe (Oxford EDX system attached to JEOL SEM JSM-5600) at Chiba University and a wavelength-dispersive type electron microprobe (JEOL JXA-8800M) at the National Institute of Polar Research. Oxide ZAF correction was applied. Synthesized oxides and natural minerals were used as standards. Representative analyses are summarized in Tables 1 and 2.

Sapphirine: X_{Mg} (= Mg/(Mg + Fe^{2+})) is 0.78. Fe^{3+} content estimated from stoichiometry is high (Fe^{3+}/total Fe is *c.* 0.3). It is poor in Si and rich not only in Fe^{3+} but also in Al as is expected, because it occurs in a silica-undersaturated and alumina-saturated system.

Spinel: Spinel shows variations in both X_{Mg} (0.44–0.52) and Zn content (up to 2 wt% ZnO), which are strongly correlated to each other. The richer in Zn, the higher in X_{Mg}. On the other hand, estimated Fe^{3+}/total Fe is almost constant (*c.* 0.1).

Cordierite: There is a small difference in X_{Mg} between cordierite in the sillimanite pseudomorphs (0.87) and that in the matrix (0.85).

Orthopyroxene: No detectable zoning is observed even in coarse grains. Al-content is *c.* 5.5 wt% Al_2O_3, and X_{Mg}= 0.71. Estimated Fe^{3+}/total Fe is almost constant (*c.* 0.1).

Phlogopite: Composition varies depending upon the associated minerals and the mode of occurrence. Phlogopite in the sillimanite pseudomorphs is richest in Ti as is expected, because it coexists with rutile. Retrograde phlogopite formed after orthopyroxene is poor in Ti compared to nearby coarse primary phlogopite in the matrix. On the other hand, all grains are poor in both F and Cl (< 1 wt%) .

Table 1. Representative EPMA analyses of minerals in sillimanite pseudomorphs after andalusite and surrounding coronas.

Mineral	Spr				Spl			Crd			Phl	Sil	Crn	Rt
Anal. Pt. No.	1	2	74	75	4	24	35	77	15	26	F-3	6	27	21
SiO_2	12.27	12.03	12.35	11.86	0.00	0.04	0.00	49.54	49.27	49.13	36.74	36.82	0.03	0.00
TiO_2	0.04	0.07	0.05	0.05	0.00	0.04	0.00	0.00	0.00	0.00	3.43	0.06	0.04	96.35
Al_2O_3	62.13	62.13	61.35	62.37	60.97	62.28	62.29	33.35	33.22	32.97	17.97	61.40	98.82	0.02
Cr_2O_3	0.06	0.01	0.02	0.00	0.00	0.00	0.00	0.00	0.00	0.00	0.00	0.00	0.00	0.08
FeO*	10.73	10.42	10.68	10.29	28.20	24.71	22.82	3.09	3.45	3.61	10.36	0.84	0.80	0.90
MnO	0.16	0.17	0.22	0.26	0.48	0.48	0.61	0.06	0.17	0.10	0.06	0.05	0.04	0.06
ZnO	0.10	0.01	0.09	0.00	0.55	1.13	2.04	0.00	0.00	0.07	0.06	0.00	0.03	0.05
MgO	15.10	14.97	15.15	15.02	10.82	12.10	12.47	11.91	11.37	11.24	17.14	0.03	0.00	0.00
CaO	0.01	0.02	0.00	0.00	0.00	0.01	0.01	0.02	0.04	0.02	0.00	0.02	0.01	0.03
Na_2O	0.00	0.01	0.03	0.00	0.04	0.00	0.00	0.17	0.22	0.14	0.22	0.02	0.02	0.03
K_2O	0.00	0.00	0.00	0.00	0.00	0.00	0.00	0.00	0.00	0.00	9.52	0.00	0.00	0.00
P_2O_5	0.02	0.03	0.00	0.00	0.04	0.00	0.01	0.00	0.03	0.02	0.01	0.00	0.00	0.03
F											0.09			
Cl											0.08			
-O											-0.05			
total	100.62	99.87	99.94	99.85	101.10	100.83	100.37	98.14	97.77	97.30	95.62	99.24	99.78	97.55
O	20	20	20	20	4	4	4	18	18	18	22	5	3	2
Si	1.465	1.446	1.485	1.424	0.000	0.000	0.000	4.993	4.995	5.006	5.352	1.005	0.001	0.000
Ti	0.004	0.006	0.005	0.005	0.000	0.001	0.000	0.000	0.000	0.000	0.376	0.001	0.000	0.993
Al	8.741	8.797	8.695	8.825	1.918	1.942	1.947	3.961	3.969	3.959	3.085	1.976	1.990	0.000
Cr	0.006	0.001	0.002	0.000	0.000	0.000	0.000	0.000	0.000	0.000	0.000	0.000	0.000	0.001
Fe^{3+}**	0.317	0.300	0.324	0.317	0.082	0.056	0.053							
Fe^{2+}**	0.754	0.746	0.745	0.716	0.548	0.491	0.454							
Fe*								0.260	0.292	0.308	1.262	0.019	0.011	0.010
Mn	0.016	0.017	0.022	0.026	0.011	0.011	0.014	0.005	0.015	0.009	0.007	0.001	0.001	0.001
Zn	0.009	0.001	0.008	0.000	0.011	0.022	0.040	0.000	0.000	0.005	0.006	0.000	0.000	0.001
Mg	2.686	2.680	2.714	2.687	0.430	0.477	0.493	1.789	1.718	1.708	3.722	0.001	0.000	0.000
Ca	0.001	0.003	0.000	0.000	0.000	0.000	0.000	0.002	0.004	0.002	0.000	0.001	0.000	0.000
Na	0.000	0.003	0.000	0.000	0.000	0.000	0.000	0.032	0.043	0.028	0.061	0.001	0.001	0.001
K	0.000	0.000	0.000	0.000	0.000	0.000	0.000	0.000	0.000	0.000	1.769	0.000	0.000	0.000
P	0.000	0.000	0.000	0.000	0.000	0.000	0.000	0.000	0.003	0.002	0.001	0.000	0.000	0.000
F								0.000	0.000	0.000	0.039	0.000	0.000	0.000
Cl								0.000	0.000	0.000	0.020	0.000	0.000	0.000
total	13.999	14.000	14.000	14.000	3.000	3.000	3.001	11.042	11.039	11.027	15.641	3.005	2.004	1.007
$Mg/Mg+Fe^{2+}$	0.781	0.782	0.785	0.790	0.440	0.493	0.521	0.873	0.855	0.847	0.747			
Fe^{3+}/total Fe	0.296	0.287	0.303	0.307	0.130	0.102	0.105							

* Total Fe

** Fe^{2+} and Fe^{3+} were calculated assuming ideal stoichiometry.

Table 2. Representative EPMA analyses of minerals in the matrix of Sp. 99082501X.

Mineral	Opx			Crd		Phl				Pl				
Anal. Pt. No.	53	87	88	81	95	F-14	F-11	F-12	F-26	41	45	91	92	94
SiO_2	50.06	51.11	51.09	48.93	49.27	37.58	38.29	38.32	38.42	63.22	68.80	59.80	60.32	61.15
TiO_2	0.05	0.03	0.02	0.00	0.00	3.05	1.15	1.01	0.84	0.00	0.05	0.01	0.03	0.01
Al_2O_3	5.44	5.46	5.58	32.88	33.13	16.68	16.33	16.56	16.65	22.56	19.27	24.78	24.79	24.45
Cr_2O_3	0.00	0.00	0.00	0.03	0.00	0.02	0.00	0.00	0.00	0.03	0.01	0.00	0.00	0.00
FeO*	19.17	19.23	19.70	3.72	3.53	11.88	9.91	9.64	9.67	0.11	0.12	0.04	0.00	0.09
MnO	0.67	0.64	0.66	0.14	0.03	0.05	0.04	0.09	0.11	0.00	0.00	0.00	0.00	0.01
ZnO	0.12	0.03	0.01	0.00	0.01	0.00	0.01	0.00	0.04	0.00	0.03	0.00	0.10	0.05
MgO	23.63	23.99	23.63	11.00	11.16	16.22	18.59	18.67	19.00	0.01	0.03	0.00	0.00	0.01
CaO	0.10	0.10	0.08	0.02	0.00	0.00	0.01	0.00	0.00	3.93	0.39	6.36	6.68	5.87
Na_2O	0.01	0.00	0.00	0.20	0.14	0.22	0.21	0.25	0.19	9.12	11.38	8.01	7.68	8.31
K_2O	0.00	0.00	0.00	0.00	0.00	9.32	8.94	9.07	8.93	0.11	0.04	0.14	0.18	0.07
P_2O_5	0.00	0.02	0.00	0.00	0.02	0.00	0.03	0.00	0.00	0.09	0.03	0.04	0.00	0.05
F						0.08	0.12	0.11	0.10					
Cl						0.10	0.03	0.07	0.11					
-O						-0.06	-0.06	-0.06	-0.07					
total	99.24	100.61	100.77	96.92	97.29	95.14	93.59	93.72	93.99	99.18	100.15	99.18	99.78	100.06
O	6	6	6	18	18	22	22	22	22	8	8	8	8	8
Si	1.846	1.858	1.858	5.008	5.013	5.527	5.646	5.642	5.637	2.813	3.000	2.684	2.691	2.715
Ti	0.001	0.001	0.001	0.000	0.000	0.337	0.127	0.112	0.093	0.000	0.002	0.000	0.001	0.000
Al	0.236	0.234	0.239	3.966	3.973	2.891	2.838	2.873	2.879	1.183	0.990	1.311	1.304	1.280
Cr	0.000	0.000	0.000	0.002	0.000	0.002	0.000	0.000	0.000	0.001	0.000	0.000	0.000	0.000
Fe^{3+} **	0.070	0.049	0.044											
Fe^{2+} **	0.521	0.535	0.555											
Fe*				0.318	0.300	1.461	1.222	1.186	1.186	0.004	0.004	0.002	0.000	0.003
Mn	0.021	0.020	0.020	0.012	0.003	0.006	0.005	0.011	0.014	0.000	0.000	0.000	0.000	0.000
Zn	0.003	0.001	0.000	0.000	0.001	0.000	0.001	0.000	0.004	0.000	0.001	0.000	0.003	0.002
Mg	1.298	1.299	1.280	1.678	1.693	3.557	4.087	4.098	4.156	0.001	0.002	0.000	0.000	0.001
Ca	0.004	0.004	0.003	0.002	0.000	0.000	0.002	0.000	0.000	0.187	0.018	0.306	0.319	0.279
Na	0.000	0.000	0.000	0.040	0.028	0.063	0.060	0.071	0.054	0.787	0.962	0.697	0.664	0.715
K	0.000	0.000	0.000	0.000	0.000	1.749	1.682	1.703	1.671	0.006	0.002	0.008	0.010	0.004
P	0.000	0.000	0.000	0.000	0.001	0.000	0.004	0.000	0.000	0.003	0.001	0.002	0.000	0.002
F						0.037	0.056	0.051	0.046					
Cl						0.025	0.007	0.017	0.027					
total	4.000	4.001	4.000	11.026	11.012	15.593	15.674	15.696	15.694	4.985	4.982	5.010	4.992	5.001
$Mg/(Mg+Fe^{2+})$	0.714	0.708	0.698	0.841	0.849	0.709	0.770	0.776	0.778					
Fe^{3+}/total Fe	0.118	0.084	0.073											
an										0.191	0.018	0.303	0.321	0.280
ab										0.803	0.980	0.689	0.669	0.716
or										0.006	0.002	0.008	0.010	0.004

* Total Fe

** Fe^{2+} and Fe^{3+} were calculated assuming ideal stoichiometry.

Plagioclase: Coarse grains show weak normal zoning; An content decreases from *c.* 32 mole % at the core to 28 mole % at the rim. Albite (An content is up to 2 mole %) is occasionally found within and around dusty inclusions in interstitial-type plagioclase grains. The dusty inclusions may be mixtures of several clay minerals, because SiO_2, Al_2O_3, FeO*, MgO, CaO, Na_2O, K_2O and P_2O_5 are present as major elements (> 1 wt%).
Other minerals (sillimanite, corundum, rutile, ilmenite): Sillimanite and corundum contain up to 1 wt% Fe_2O_3. Rutile may contain some minor elements such as Nb and U, because yellow pleochroic halos are usually observed around rutile grains in cordierite.

5. Discussion

5.1. P-T path followed by granulites

The occurrence of sillimanite pseudomorphs after andalusite porphyroblasts definitely indicates the prograde *P-T* path followed by the rock from the andalusite to the sillimanite stability fields. Similar sillimanite pseudomorphs after andalusite were reported from the Valriver area to the north of the Dabeeb-Hytkoras area (Raith and Harley, 1998). The pseudomorphs there occur in the quartz-plagioclase ± garnet matrix and are surrounded by coronas of garnet, and therefore are distinctly different from those of the present case. It is not known at present whether the different coronas surrounding sillimanite pseudomorphs resulted from different *P-T* paths of granulites in the two areas or from different bulk rock compositions. The observed mineral assemblage sillimanite + corundum + cordierite + spinel + sapphirine + rutile in the sillimanite pseudomorphs is univariant in the system FeO-MgO-Al_2O_3-SiO_2-TiO_2, and may be useful to put constraints on the *P-T* path of the rock. The following mineral assemblages have also been reported in Mg-Al-rich rocks from outcrops around K2 of Waters and Moore (1985) in the Dabeeb-Hytkoras area (Waters, 1986b; Hokada *et al.*, 2001; this study).

(1) Corundum + sillimanite + cordierite + sapphirine + spinel + phlogopite,
(2) Corundum + sillimanite + cordierite + sapphirine + orthopyroxene + phlogopite,
(3) Cordierite + sapphirine + spinel + orthopyroxene + phlogopite,
(4) Cordierite + spinel + garnet + orthopyroxene + phlogopite,
(5) Sillimanite + cordierite + garnet + phlogopite,
(6) Cordierite + spinel + garnet + phlogopite.

Some of the said mineral assemblages additionally contain kornerupine, tourmaline and/or plagioclase. The relevant partial petrogenetic grid in the system FeO-MgO-Al_2O_3-SiO_2 is shown in Fig. 8. Invariant points I_1 and I_2 in Fig. 8 have been well constrained experimentally and theoretically. I_1 may be located at about 1050°C and 11 kbar, while I_2 is at about 950°C and 9 kbar (Spear, 1993). The invariant point I_3 (qtz, grt) in Fig. 8 was proposed by Waters (1986b) and may be located on the lower-pressure and lower-temperature side of I_2. Mineral assemblages (1) and (2) are univariant in the system and correspond to univariant lines labeled (qtz, grt, opx) and (qtz, grt, spl) emanating from I_3. It is probable that the retrograde *P-T* path followed by the rocks is characterized by isobaric cooling as proposed by Waters (1989) (Fig. 8), because both univariant lines (qtz, grt, opx) and (qtz, grt, spl) have small d*P*/d*T*, as calculated by Kriegsman and Schumacher (1999).

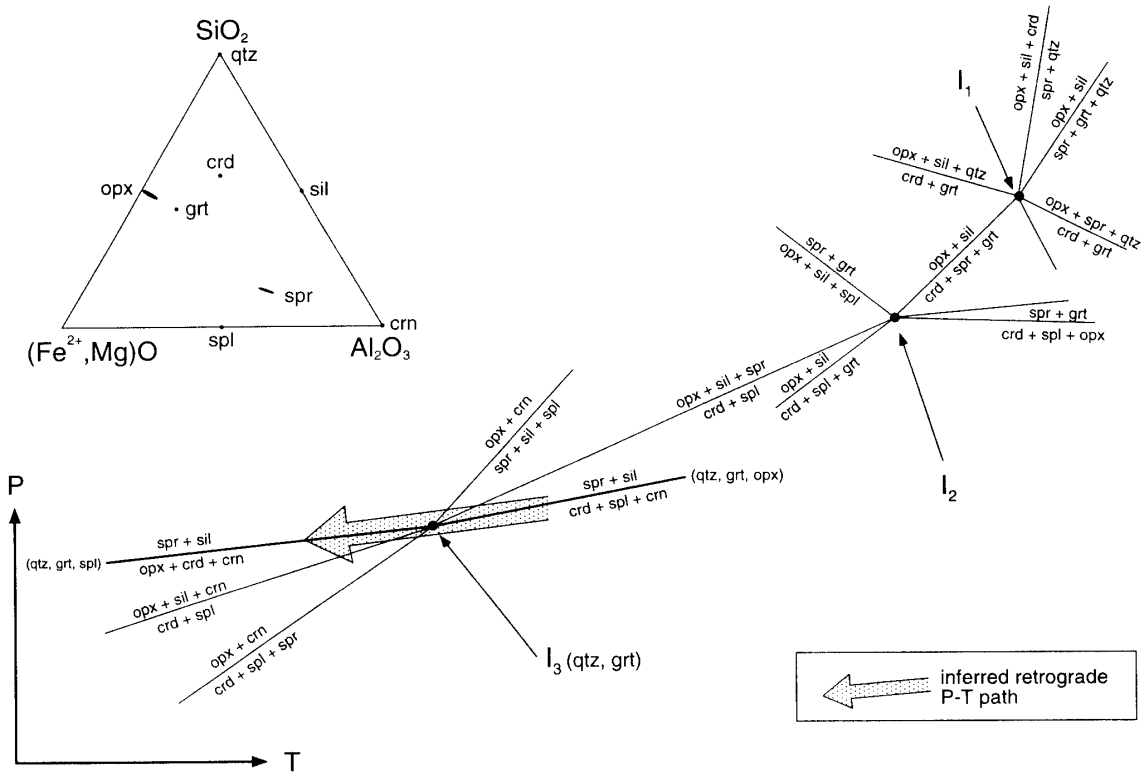

Fig. 8. Partial petrogenetic grid in the system FeO-MgO-Al_2O_3-SiO_2. Invariant points I_1 and I_2 are after Spear (1993), and invariant point I_3 is after Waters (1986b). Inferred nearly isobaric cooling path is also shown.

5.2. Partial melting and origin of Mg-Al-rich rocks

Since Eskola's (1914) classic study, Mg-Al-rich rocks such as cordierite-anthophyllite schists, cordierite-orthopyroxene gneisses and cordierite-phlogopite gneisses have been given special attention for both historical and petrologic reasons (Spear, 1993). Their bulk compositions do not correspond to any commonly occurring igneous or sedimentary protoliths. Many origins have been proposed for Mg-Al-rich rocks. The three major hypotheses include (1) metasomatism accompanying metamorphism; (2) a residuum of a partial melt; and (3) premetamorphic alteration by weathering, deuteric alteration by late-stage magmatic fluids or hydrothermal alteration by seawater (Spear, 1993). There have been similar debates concerning the origin of Mg-Al-rich rocks in the western Namaqualand Metamorphic Complex. Clifford *et al.* (1975a, b, 1981) interpreted and modeled them as restites after removal of 70–80% granitic liquid from precursor argillites during granulite-facies metamorphism. Later, Waters and Moore (1985), Waters (1986b) and Moore and Waters (1990) criticized the interpretation of Clifford *et al.* (1975a, b, 1981) and proposed that they are derived isochemically from sedimentary precursor based on the close field associations of the Mg-Al-rich rocks with mafic rocks and the overall geochemical trends and comparison between amphibolite- and granulite-facies samples.

The study rock is divided into two different portions: silica-undersaturated sillimanite pseudomorphs and the silica-saturated matrix (Fig. 4). Therefore, we have to

answer the question how and when the rock was divided into the two portions.

The occurrence of phlogopite + quartz symplectites after orthopyroxene in the matrix suggests the following retrograde reaction.

$$\text{Orthopyroxene} + \text{K-feldspar} + H_2O \rightarrow \text{phlogopitz} + \text{quartz}. \quad (1)$$

However, reaction (2) is more plausible than reaction (1) for the following reasons.

$$\text{Orthopyroxene} + \text{granitic melt} \rightarrow \text{phlogopite} + \text{quartz} + \text{plagioclase}. \quad (2)$$

(i) Part of the plagioclase occurs as grains containing fine-grained phlogopite and quartz (Fig. 7a, b), which are the product of reaction (2).

(ii) The modes of occurrence of quartz suggest that quartz is of retrograde origin and, therefore, there is a possibility that quartz was absent at the metamorphic peak. In the absence of quartz, cordierite-phlogopite parageneses are stable throughout the western Namaqualand Metamorphic Complex with the exception of the extremely high temperature area, where hercynitic spinel + quartz and rare osumilite-bearing assemblages occur in metapelites and the following reaction is observed (Waters, 1986a, 1989, 1991)

$$\text{Cordierite} + \text{biotite} \rightarrow \text{orthopyroxene} + \text{spinel} + \text{K-feldspar} + H_2O. \quad (3)$$

(iii) K-feldspar is completely absent in the rock. It is unlikely that all K-feldspar in the rock was consumed by retrograde reaction (1). On the other hand, it is highly plausible that granitic melt produced by partial melting was removed from the rock, leaving no K-feldspar.

Thus it is inferred that granitic melt was present in the matrix at the thermal peak, which, in turn, suggests that the dehydration melting reaction (4) (reverse reaction of reaction (2)) took place at prograde to peak metamorphic stages.

$$\text{Phlogopite} + \text{quartz} + \text{plagioclase} \rightarrow \text{orthopyroxene} + \text{granitic melt}. \quad (4)$$

The spinel-cordierite coronas surrounding sillimanite pseudomorphs are indicative of reactions between sillimanite and the matrix minerals, especially phlogopite (see Figs. 3 and 4a).

$$\text{Sillimanite} + \text{phlogopite} \rightarrow \text{spinel} + \text{cordierite} + \text{K-feldspar} + H_2O. \quad (5)$$

However, reaction (6) is more likely than reaction (5) for the following reasons.

$$\text{Sillimanite} + \text{granitic melt} \rightarrow \text{cordierite} + \text{spinel} + \text{sapphirine} + \text{corundum}. \quad (6)$$

(i) K-feldspar, which should be produced by reaction (5), is completely absent in the rock.

(ii) Dehydration melting reaction (4) to produce granitic melt is inferred to have taken place in the rock, as discussed above.

(iii) The occurrence of corundum in addition to spinel and cordierite in the coronas implies a silica-undersaturated environment, which is likely to appear during partial melting of relatively silica-poor rocks.

(iv) The observed coronas are identical with those commonly observed around Al_2SiO_5 xenocrysts in andesitic to rhyolitic magmas.

In summary, mineral textures strongly suggest the presence of granitic melt at the thermal peak in the rock. The absence of K-feldspar and the depletion in the granitic component suggest that the geochemical character of the rock can be attributed, at least partly, to partial melting and extraction of the produced granitic melt. The degree of partial melting and amount of removed melt, however, are not known at present. In this connection, the intimate field relations between Mg-Al-rich rocks and basic rocks and geochemical features pointed out by Waters and Moore (1985), Waters (1986a, b) and Moore and Waters (1990) may be significant.

The dusty interiors of interstitial-type plagioclase grains may be a mixture of clay minerals, as mentioned above. However, neither surface weathering nor low-temperature hydrothermal alteration explain the occurrence of such material enclosed by fresh plagioclase mantles in the fresh rock where cordierite shows little sign of alteration to pinite (Fig. 7c). There is a possibility that the dusty interiors of interstitial-type plagioclase grains were trapped hydrous melt.

6. Conclusions

We found cordierite-phlogopite gneiss carrying sillimanite pseudomorphs after andalusite from the granulite-facies Dabeeb-Hytkoras area in the western Namaqualand Metamorphic Complex. It confirms the prograde *P-T* path of the rock from the andalusite to the sillimanite stability fields. In addition, the mineral assemblages in Mg-Al-rich rocks suggest a subsequent isobaric cooling path. The observed mineral textures are most satisfactorily explained by the presence of granitic melt in the rock at the thermal peak and its removal. Thus, the Mg-Al-rich geochemical character of the rock can be attributed to, at least partly, partial melting and extraction of produced granitic melt.

Acknowledgments

This study was supported mainly by a Grant-in-Aid for Scientific Research from the Japanese Ministry of Education, Science, Sports and Culture to K. Shiraishi (No. 0904116). Part of the analytical work was supported by a Grant-in-Aid for Scientific Research from the Japanese Ministry of Education, Science, Sports and Culture to Y. Hiroi (No. 10304042).

References

Andreoli, M.A.G., Smith, C.B., Watkeys, M., Moore, M.J., Ashwal, L.D. and Hart, R.J. (1994): The geology of the Steenkampskraal monazite deposit, South Africa: Implication for REE-Th-Cu mineralization in charnockite-granulite terranes. Econ. Geol., **89**, 994–1016.

Clifford, T.N., Gronow, J., Rex, D.C. and Burger, A.J. (1975a): Geochronology and petrogenetic studies of high-grade metamorphic rocks and intrusives in Namaqualand, South Africa. J. Petrol., **16**, 154–188.

Clifford, T.N., Stumpfl, E.F. and McIver, J.R. (1975b): A sapphirine-cordierite-bronzite-phlogopite paragneiss from Namaqualand, South Africa. Mineral. Mag., **40**, 347–356.

Clifford, T.N., Stumpfl, E.F., Burger, A.J. , McCarthy, T.S. and Rex, D.C. (1981): Mineral-chemical and isotopic studies of Namaqualand granulites, South Africa: a Grenville analogue. Contrib.

Mineral. Petrol., **77**, 225–250.

Clifford, T.N., Barton, E.S., Retief, E.A., Rex, D.C. and Fanning, C.M. (1995): A crustal progenitor for the intrusive anorthosite-charnockite kindred of the cupriferous Koperberg Suite, O'okiep District, Namaqualand, South Africa; new isotope data for the country rocks and the intrusives. J. Petrol., **36**, 231–258.

Eskola, P. (1914): On the petrology of Orijarvi region, southwest Finland. Bull. Comm. Geol. Finl., **40**, 277.

Hokada, T., Motoyoshi, Y., Hiroi, Y., Shimura, T., Yuhara, M., Shiraishi, K., Grantham, G.H. and Knoper, M.W. (2001): Petrography and mineral chemistry of high-grade pelitic gneisses and related rocks from Namaqualand, South Africa. Mem. Natl Inst. Polar Res., Spec. Issue, **55**, 105–126.

Jacobs, J., Thomas, R.J. and Weber, K. (1993): Accretion and indentation tectonics at the southern edge of the Kaapvaal craton during the Kibaran (Grenville) orogeny. Geology, **21**, 203–206.

Joubert, P. (1971): The regional tectonism of the gneisses of part of Namaqualand. Bull. Precambrian Res. Unit, Univ. Cape Town, **10**, 220 p.

Joubert, P. (1986a): Namaqualand - a model of Proterozoic accretion. Trans. Geol. Soc. S. Afr., **89**, 79–96.

Joubert, P. (1986b): The Namaqualand Metamorphic Complex - a summary. Mineral Deposits of South Africa, Vol. 2, ed. by C.R. Anhaeusser and S. Maske. Johannesburg, Geol. Soc. S. Afr., 1395–1420.

Kriegsman, L.M. and Schumacher, J.C. (1999): Petrology of sapphirine-bearing and associated granulites from central Sri Lanka. J. Petrol., **40**, 1211–1239.

Moore, J.M. (1989): A comparative study of metamorphosed supracrustal rocks from the western Namaqualand Metamorphic Complex. Bull. Precambrian Res. Unit, Univ. Cape Town, **37**, 370 p.

Moore, J.M. and Waters, D.J. (1990): Geochemistry and origin of cordierite-orthoamphibole/orthopyroxene-phlogopite rocks from Namaqualand, South Africa. Chem. Geol., **85**, 77–100.

Nowicki, T.E., Frimmel, H.E. and Waters, D.J. (1995): The occurrence of osumilite in pelitic granulites of the Namaqualand metamorphic complex, South Africa. S. Afr. J. Geol., **98**, 191–201.

Raith, J.G. and Harley, S.L. (1998): Low-P/high-T metamorphism in the Okiep Copper District, western Namaqualand, South Africa. J. Metamorph. Geol., **16**, 281–305.

Robb, L.J., Armstrong, R.A. and Waters, D.J. (1999): The history of granulite-facies metamorphism and crustal growth from single zircon U-Pb geochronology: Namaqualand, South Africa. J. Petrol., **12**, 1747–1770.

Rosenfeld, J.L. (1969): Stress effects around quartz inclusions in almandine and the piezothermometry of coexisting aluminum silicates. Am. J. Sci., **267**, 317–351.

Spear, F. (1993): Metamorphic Phase Equilibria and Pressure-Temperature-Time Paths. Washington, D.C., Mineralogical Society of America, 799 p.

Thomas, R.J., Agenbachat, A.L.D., Cornell, D.H. and Moore, J.M. (1994): The Kibaran of South Africa: Tectonic evolution and metallogeny. Ore Geol. Rev., **9**, 131–160.

Waters, D.J. (1986a): Metamorphic zonation and thermal history of pelitic gneisses from western Namaqualand, S. Africa. Trans. Geol. Soc. S. Afr., **89**, 97–102.

Waters, D.J. (1986b): Metamorphic history of sapphirine-bearing and related magnesian gneisses from Namaqualand, South Africa. J. Petrol., **27**, 541–565.

Waters, D.J. (1988): Partial melting and the formation of granulite facies assemblages in Namaqualand, South Africa. J. Metamorph. Geol., **6**, 387–404.

Waters, D.J. (1989): Metamorphic evidence for the heating and cooling path of Namaqualand granulites. Evolution of Metamorphic Belts, ed. by J.S. Daly *et al.* Oxford, Blackwell, 357–363 (Spec. Publ., Geol. Soc., 43).

Waters, D.J. (1990): Thermal history and tectonic setting of the Namaqualand granulites, southern Africa: clues to Proterozoic crustal development. Granulites and Crustal Evolution, ed. by D. Vielzeuf and Ph. Vidal. Dordrecht, Kluwer Academic, 243–256.

Waters, D.J. (1991): Spinel-quartz granulites: phase relations, and implications for crustal processes. Eur. J. Mineral., **3**, 367–386.

Waters, D.J. and Moore, J.M. (1985): Kornerupine in Mg-Al-rich gneisses from Namaqualand, South Africa: mineralogy and evidence for late-metamorphic fluid activity. Contrib. Mineral. Petrol., **91**, 369–382.

Waters, D.J. and Whales, C.J. (1984): Dehydration melting and the granulite transition in metapelites from southern Namaqualand, S. Africa. Contrib. Mineral. Petrol., **88**, 269–275.

Zelt, G.A. (1980): Granulite-facies metamorphism in Namaqualand, South Africa. Precamb. Res., **13**, 253–274.

(Received January 12, 2001; Revised manuscript accepted May 25, 2001)